Available online at www.sciencedirect.com
ScienceDirect
Journal of the European Ceramic Society 29 (2009) 3045–3052
www.elsevier.com/locate/jeurceramsoc

Effect of ZnO on the structure, microstructure and electrical properties of KNN-modified piezoceramics

F. Rubio-Marcos *, J.J. Romero, M.G. Navarro-Rojero, J.F. Fernandez

Electroceramic Department, Instituto de Cerámica y Vidrio, CSIC, Kelsen 5, 28049 Madrid, Spain

Received 10 February 2009; received in revised form 9 April 2009; accepted 22 April 2009
Available online 30 May 2009

Abstract

The effects of ZnO addition on structure, microstructure and dielectric properties of $(K_{0.44}Na_{0.52}Li_{0.04})(Nb_{0.86}Ta_{0.10}Sb_{0.04})O_3$ ceramics (KNL–NTS) are investigated. Doping provokes phase segregation, evidenced by the appearance of different types of grains and a tetragonal tungsten–bronze secondary phase at high ZnO doping levels. A clear increase of ferroelectric–paraelectric and orthorhombic-to-tetragonal phase transition temperatures with ZnO content is observed. This produces a reduction of the room temperature piezoelectric constants due to the reduction of the tetragonality (*c*/*a*) ratio of the KNL–NTS structure.

Keywords: A. Grain growth; B. Microstructure-final; C. Piezoelectric properties; D. Perovskites; E. Actuators

1. Introduction

Lead zirconate titanate (PZT) family ceramics are the most widely used piezoelectric materials to date, due to their high piezoelectric response, large scale production capability and the tailoring of their properties through composition. Recently, the European Union has published a health normative (ROHS)[1] avoiding the use of lead on any manufactured item due to its toxicity and environment risks. Nevertheless, piezoelectric PZT ceramics are out of this normative due to the lack of an adequate alternative. One promising alternative is the family formed by materials based on potassium sodium niobate solid solutions (KNN), due to their good electromechanical properties.[2,3] High attention is paid to find adequate compositions and processing procedures to obtain competitive and reliable piezoelectric materials. There are currently some alternatives to PZT ceramics for sensor applications, as for instance the PVDF, but there are no feasible lead free piezoceramics for power applications up to now.

KNN-based ceramics show sintering difficulties and exhibit deliquescence when they are exposed to moisture.[4] In order to solve the densification problems, different advanced processes such as spark plasma sintering[5] or hot pressing[6] were developed to promote the sintering, which lead to the enhancement of both the density and the related properties. However, these processes are not suitable for massive production of piezoceramics with different shapes. The sinterability of these materials can also be improved by using different compounds as sintering promoters, such as CuO,[7,8] SnO_2[9] and MnO.[10] The sintering promoters usually enter in B position of the ABO_3 perovskite structure and produce A site vacancies that suppress the formation of the hygroscopic secondary products.[11]

Recently, Ochoa et al.[12] studied the feasibility of the $(K,Na,Li)(Nb,Ta,Sb)O_3$ system for its use in transducers and the results showed that the behaviour of the system was similar to other perovskite-type piezoceramics. The higher contribution to the dielectric, piezoelectric and elastic material responses were fundamentally related to extrinsic effects. The dielectric and mechanical losses at room temperature were similar to a soft PZT ceramic and too high to be used in power devices. Doping is usually recognized as a method to reduce the dielectric and mechanical losses of piezoelectric ceramics and ZnO has been successfully used to reduce the dielectric losses in different materials.[13,14] In particular, ZnO has been previously used on KNN in an attempt to reduce the dielectric losses of the material.[15] It has been shown that addition of ZnO helps to

* Corresponding author.
E-mail address: frmarcos@icv.csic.es (F. Rubio-Marcos).

0955-2219/$ – see front matter © 2009 Elsevier Ltd. All rights reserved.
doi:10.1016/j.jeurceramsoc.2009.04.026

increase the density of the material and avoids the deliquescence.

The purpose of this work is to investigate the effect of ZnO doping on the structure, microstructure and electrical properties of $(K_{0.44}Na_{0.52}Li_{0.04})(Nb_{0.86}Ta_{0.10}Sb_{0.04})O_3$ piezoceramics.

2. Experimental

$(K_{0.44}Na_{0.52}Li_{0.04})(Nb_{0.86}Ta_{0.10}Sb_{0.04})O_3$, KNL–NTS, ceramics were synthesized by conventional solid-state sintering processes. The raw materials used in this study are potassium carbonate (K_2CO_3, 99.0%), sodium carbonate (Na_2CO_3, 99.5%), lithium carbonate (Li_2CO_3, 99.5%), niobium oxide (Nb_2O_5, 99.5%), tantalum oxide (Ta_2O_5, 99.0%), antimonium oxide (Sb_2O_5, 99.995%) and zinc oxide (ZnO, 99.7%). The raw materials were milled individually, in order to obtain an appropriate distribution of the particle size.[16] The proper amounts of milled powders were mixed and attrition-milled using ZrO_2 balls in ethanol medium for 3 h, dried and calcined at 700 °C for 2 h. The materials obtained were composed of particles with a narrow size distribution around 350 nm, formed by agglomerated nanometer-size particles. This small particle size was attributed to the low temperature process which improves the reactivity of the powders. Recent studies on the reactivity of the sodium potassium niobates reveal that the perovskite structure is formed at temperatures near 700 °C,[17] although the regular synthesis process of KNN in the literature uses higher temperatures.

The compositions with 0.1, 0.3, 0.5 and 1.0 wt% of ZnO were prepared by incorporating the appropriate amounts of ZnO to a dispersion of calcined KNL–NTS in ethanol by a high shear mixing process at 6000 rpm. After the mixing step, the powders were oven-dried and then sieved and pressed at 200 MPa into disks of 10 mm in diameter and 0.7 mm in thickness. The pellets were sintered in air at 1125 °C for 16 h. The density of the sintered samples was measured using the Archimedes method. For the electrical measurements, a fired silver paste was used for the electric contacts. The samples were poled in a silicon oil bath at 25 °C by applying a direct current electric field of 4.0 kV/mm during 30 min.

The crystalline symmetry was examined by X-ray diffraction analysis (XRD, Siemens D5000, Munich, Germany, Cu Kα radiation) using Si as internal standard. The lattice parameters were refined by a global simulation of the full diagram using the *fullprof* program.[18] Microstructure was evaluated on polished and thermally etched samples (1000 °C for 5 min) using a Field Emission Scanning Electron Microscope, FE-SEM (Hitachi S-4700, Tokio, Japan), equipped with energy dispersive spectroscopy, EDS. The average grain size was determined from FE-SEM micrographs by an image processing and analysis program (Leica Qwin, Leica Microsystems Ltd., Cambridge, England) considering more than 500 grains in each measurement.

The temperature dependence of the ceramics permittivity was measured using an impedance analyzer (HP4294A, Agilent Technologies Inc., Santa Clara, CA) in the frequency range of 100 Hz–1 MHz and the temperature range of 30–600 °C, at 2 °C/min. P–E hysteresis loops were determined by a Radiant Technologies Inc. hysteresis meter (RT 6000 HVS) at room temperature. The piezoelectric constant d_{33} was measured using a piezo-d_{33} meter (YE2730A d_{33} Meter, APC International, Ltd., USA). The electromechanical coupling factor k_p was determined at room temperature by resonance and antiresonance methods on the basis of IEEE standards.

3. Results and discussion

3.1. Structure and microstructure evolution

Fig. 1 shows the density variation of KNL–NTS as a function of the ZnO content for samples sintered at 1125 °C for 16 h. When increasing ZnO content, the bulk density decreases from 4.69 ± 0.01 g/cm^3 for samples without ZnO to 4.57 ± 0.02 g/cm^3 for 1 wt% of ZnO.

Fig. 2(a) shows the XRD patterns of the ceramics with different ZnO contents. In addition to the perovskite structure, secondary phases were found in samples with ZnO content higher than 0.3 wt%. All the ceramics possess a perovskite structure in which the tetragonal symmetry is dominant at room temperature, though a slight increase of the orthorhombic symmetry is observed with increasing ZnO content. The secondary crystalline phase could be assigned to $K_3LiNb_6O_{17}$[19] (KLN) or $K_6Nb_{10.88}O_{30}$ (PDF#87-1856), both with tungsten–bronze type structure. KLN is a transparent oxide with space group P4bm (point group: 4 mm), and a ferroelectric–paraelectric phase transition[20] temperature of ~420 °C.

Fig. 2(b) shows a magnification of the (2 0 0) and (0 0 2) peaks of the XRD patterns for KNL–NTS ceramics as a function of the ZnO content. It is clear that the perovskite structure with tetragonal symmetry predominates in all samples. To calculate the tetragonality ratio (*c*/*a*) and the unit cell volume, the whole XRD pattern was refined with a *fullprof* program,[18] constraining the refinement to point group P4mm, a primitive polar tetragonal unit cell. The samples show slight evolution of the tetragonal (0 0 2) and (2 0 0) diffraction peaks with increasing ZnO content. Fig. 2(c) shows the variation of the lattice parameters as a function of the ZnO content. The lattice constant *c* decreases with ZnO content, while the lattice constant *a*

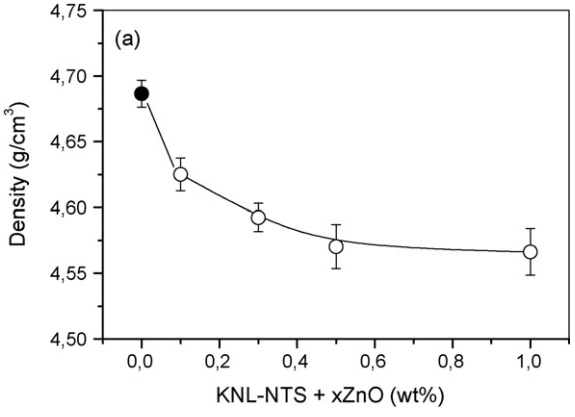

Fig. 1. Density of KNL–NTS as a function of the ZnO content for the ceramics sintered at 1125 °C for 16 h.

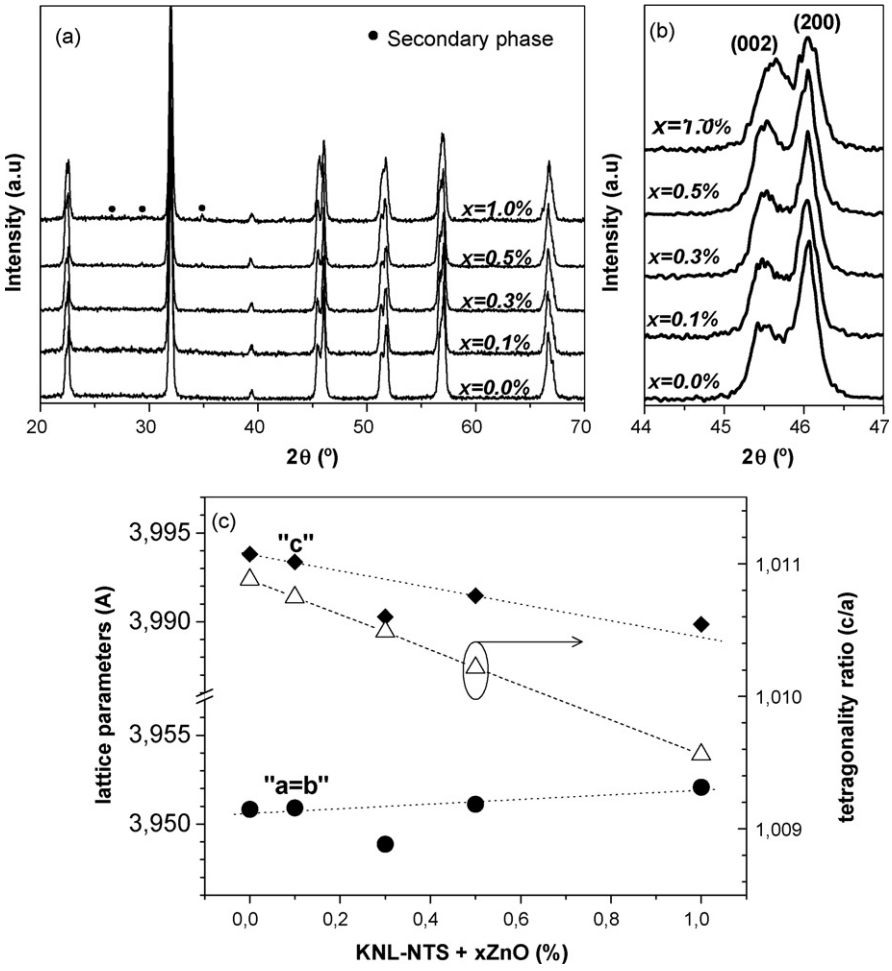

Fig. 2. (a) XRD patterns of the KNL–NTS + *x*ZnO (wt%) ceramics and (b) expansion of the 2θ region from 44° to 47°. (c) Variation of lattice parameters and tetragonality ratio, *c*/*a* (open triangles), as a function of the ZnO content.

increases. This kind of behaviour has also been reported when CuO[21] is added. The tetragonality ratio *c*/*a*, Fig. 2(c), of the ceramics decreases linearly with ZnO content. This structural evolution can be ascribed to three factors: (i) the incorporation of Zn^{2+} cations into the perovskite structure, (ii) the observed existence of a phase polymorphism on KNN-based materials composed of a main tetragonal phase and traces of a residual, low temperature orthorhombic phase[22,23] and (iii) the presence of a secondary phase, in this case the tetragonal tungsten–bronze phase observed in Fig. 2(a). The decrease in bulk density observed at high values of x ($x > 0.3$ wt%) may be attributed to the formation of the secondary phase $K_3LiNb_6O_{17}$, which possesses a lower theoretical density (~4.376 g/cm^3) than the perovskite phase.

The microstructure of the KNL–NTS ceramics as a function of the ZnO content sintered at 1125 °C for 16 h was investigated using FE-SEM. The FE-SEM micrographs, Fig. 3, showed the typical KNL–NTS morphology consisting on faceted grains with a bimodal grain size distribution. The microstructure of the undoped sample showed equiaxed grains (matrix grains) and some large, abnormal grains, square or rectangular in appearance. The microstructure of the 0.1 wt% ZnO addition sample remains nearly unaltered but for the increase of population and size of the abnormal grains. For higher ZnO contents up to a maximum 0.3 wt%, the average grain size of matrix-grains decreases significantly, while the number and size of the abnormal grains increases. Moreover, the porosity of the ceramics shows appreciable increase with the ZnO content, explaining the decrease of the samples' density as observed in Fig. 1.

The limited grain growth could be associated to two factors: (i) the existence of grains with very low curvature in spite of their low size; the straight grain boundaries are characteristic of this system in which the sintering occurs assisted by the presence of a small amount of liquid phase,[16] (ii) the effect of ZnO dopant, since the dopant is distributed during the earliest stage of sintering by vapour-phase transport and grain boundary diffusion.[13,24]

The matrix grains preserved the cubic–rectangular morphology in all samples. In contrast, the abnormal grains exhibited different morphologies. Moreover, as ZnO increases, segregated phases appear within the abnormal grains. These segregated phases increase with ZnO content. When ZnO addition reaches ≥0.3 wt%, new phases begin to appear, that can be related to the tetragonal tungsten–bronze structure seen by XRD (see Fig. 2).

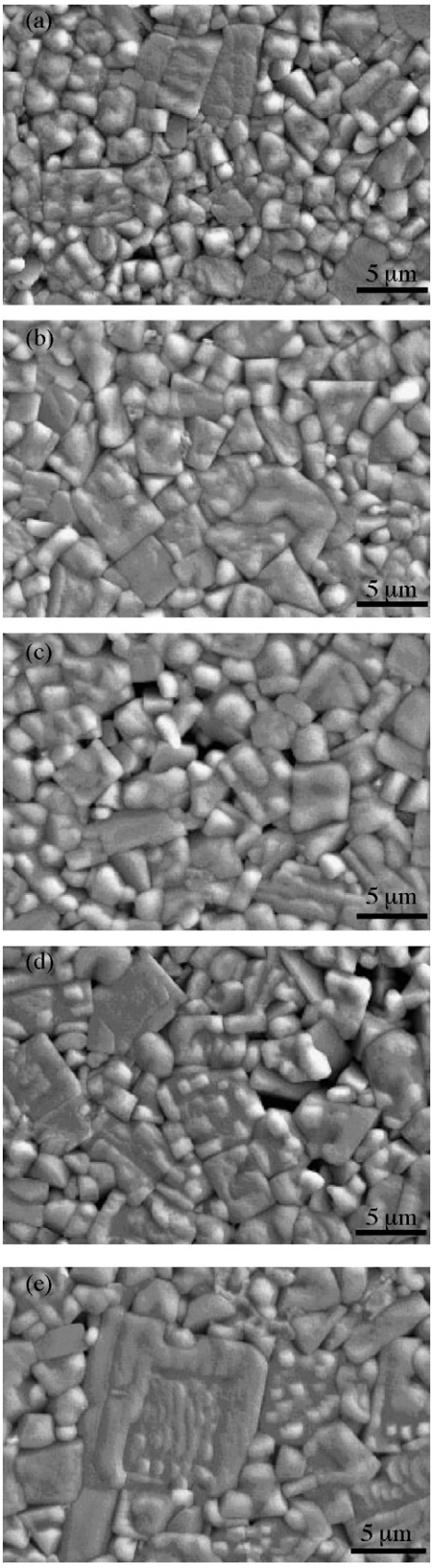

Fig. 3. Microstructure of polished and thermally etched surfaces of the KNL–NTS + xZnO (wt%) ceramics sintered at 1125 °C for 16 h. (a) Undoped, (b) $x = 0.1$, (c) $x = 0.3$, (d) $x = 0.5$ and (e) $x = 1.0$.

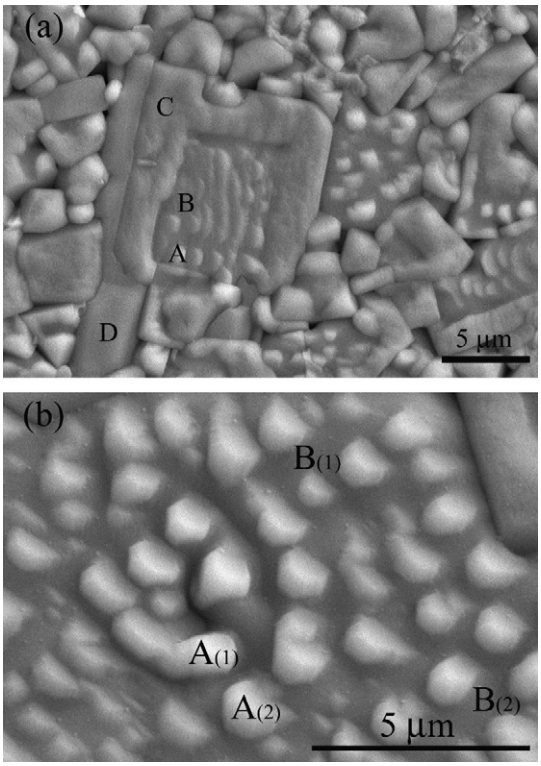

Fig. 4. Microphotographs of the KNL–NTS with the higher ZnO addition, $x = 1.00$, (a) morphology of the matrix grains, the abnormal grains and the secondary phase. (b) Magnification of the interior of an abnormal grain.

Core–shell type structure appeared in these ceramics, especially in abnormally grown grains, as shown in Fig. 4(a). This phenomenon was more relevant when the ZnO content increased. The energy dispersion spectrum analysis (EDS) revealed that the atomic percentages of elements changed within the different grain regions, as has been previously reported in KNN and other systems.[25] Table 1 lists the compositions measured by EDS on the sample with ZnO content of 1.0 wt% at the locations marked in Fig. 4(a). The results show clear differences between the different points, indicating a significant compositional segregation of the ceramics. The abnormal grains show three features that become more evident as the ZnO content increases. The core of the abnormal grains is composed of brilliant regions, with a size of ~1 μm (point A in Fig. 4(a)) surrounded by a grey matrix (point B in same figure). The grain core is surrounded by a partial shell (point C in Fig. 4(a)). This sample also shows grains with a different morphology from that of the normal KNL–NTS and abnormal grains, marked as D in Fig. 4(a). This D grain could be associated to the tungsten–bronze secondary phase observed by XRD, since the composition measured by EDS is similar to that of $Li_x(K_{0.78}Na_{0.22})_6(Nb_{0.86}Ta_{0.10}Sb_{0.04})_{10.9}O_{30}$ tungsten bronze material[26] (see Table 1). These grains show a high content of Zn^{2+} (see Table 1), indicating that the TTB phase grains are formed to accommodate the Zn^{2+} excess that cannot be incorporated on the KNL–NTS lattice. In the case of Zn-added KNN, a secondary phase corresponding to ZnO is formed for high concentrations of Zn^{2+},[15] probably because there is no alternative

Table 1
Composition on the points shown in Fig. 4(a) derived from EDS spectra.

	O	Na	K	Li	Zn	Nb	Ta	Sb	Na/K
A	58.25	16.14	6.46	–	0.15	16.68	1.62	0.70	2.50
B	62.23	10.08	5.51	–	0.12	19.46	1.77	0.83	1.82
C	61.30	8.65	8.82	–	0.00	18.93	1.77	0.54	0.98
D	63.87	2.57	9.77	–	0.53	20.53	1.74	1.00	0.26
$KNL–NTS_{nominal\ composition}$	60.00	10.40	8.80	0.80	0.00	17.2	2.00	0.80	1.18
TTB[26] $Li_x(K_{0.78}Na_{0.22})_6(Nb_{0.86}Ta_{0.10}Sb_{0.04})_{10.9}O_{30}$	63.97	2.81	9.98	–	–	19.99	2.32	0.92	0.28

crystal comprising the different components of the material that can be formed at the sintering temperature.

The described microstructures show marked compositional differences. EDS analysis of A and B regions (points A and B, Fig. 4(a)) reveals that these features possess a composition similar to the fine perovskite grains, but show a higher Na/K ratio than the expected 1.18 ratio. The possible origin of this phenomenon could be originated by the volatilization of alkali metal elements, the major drawback of KNN systems. In addition, the EDS analysis of these points revealed the presence of ZnO in the structure, suggesting that the added Zn^{2+} entered in solid solution in KNL–NTS ceramics. Fig. 4(b) shows a magnification of the A and B regions. The EDS analysis (not shown) revealed that the A-regions have a composition richer in Na^+ than B regions, showing Na/K ratios of ∼2.50 and ∼1.82, respectively, and a constant amount of Zn^{2+} cations. The Na/K ratio on these two regions is higher than the nominal 1.18 ratio of the undoped KNL–NTS ceramics. This behaviour evidences coexistence of two phases (related to a phase polymorphism): a main phase with tetragonal symmetry and a secondary phase with orthorhombic symmetry. The existence of a polymorphism in this system is a matter of controversy.[23] In this work, we show that the presence of Zn^{2+} cations stabilized the phases' coexistence. The possible origins of a polymorphism of such compounds are (i) an evolution of the grain size, (ii) an evolution of the composition and (iii) a chemical inhomogenization of the A and B perovskite ions, since the stoichiometry of these samples is very complex.

The partial shell (point C, Fig. 4(a)) has the composition of the matrix fine grains, with a Na/K concentration ratio around 0.98, similar to the characteristic ratio of the perovskite phase measured on the matrix grains. No traces of Zn^{2+} can be observed on this partial shell by EDS.

The secondary phase (point D, Fig. 4(a)) showed a Na/K concentration ratio around 0.26, much lower than the nominal ratio of 1.18. This phase is a compositional segregation previously reported in the literature.[26] The abnormally grown grain is therefore accompanied by redistribution of the related elements (specially the A-site cations) that eventually precipitate and crystallize as a secondary phase. The formation of the tungsten–bronze structure requires a large diffusion of the atoms and therefore is favoured if the samples contain ZnO. The composition of the tungsten–bronze phase can be formulated as a complex solid solution $Li_x(K_{0.78}Na_{0.22})_6(Nb_{0.86}Ta_{0.10}Sb_{0.04})_{10.9}O_{30}$, as previously described.[26]

3.2. Dielectric properties

Fig. 5(a) shows the thermal evolution of the dielectric constant (at 100 KHz) for the different compositions. As can be seen on the inset, the Curie temperature (T_c) increases almost linearly with ZnO addition, in contrast to the situation found with ZnO doped KNN.[15] This result is consistent with the change of the unit cell size indicating that the A-site replacement of Zn^{2+} increases T_c.[21] Moreover, the addition of ZnO produces a slight broadening of the transition peak and the appearance of a double peak when ZnO amount is >0.50. The second peak could be attributed to the appearance of secondary phases.

In agreement with previous works,[22] the temperature dependence of the dielectric constant for the modified-KNN systems, Fig. 5(b), shows a second transition at temperatures ranging 25–80 °C, corresponding to an orthorhombic to tetragonal phase transition ($T_{O–T}$). The temperature at which this phase transition occurs increases with the ZnO content. These shifts in the $T_{O–T}$ suggested the presence of a phase polymorphism,[22,23] where the ZnO incorporation produces a stabilization of the orthorhombic symmetry at room temperature.

It is well known that the dielectric constant of a normal ferroelectric material should follow the Curie–Weiss law when the temperature exceeds the Curie temperature. However, the dielectric constant of KNL–NTS + xZnO (wt%) ceramics obviously deviates from the Curie–Weiss law with increasing addition of ZnO. Therefore, the diffuseness of the phase transition can be determined from the modified Curie–Weiss law, $1/\varepsilon_r - 1/\varepsilon_m = C^{-1}(T - T_m)^{\gamma}$,[27] where $\gamma = 2$ corresponds to a relaxor behaviour and $\gamma = 1$ corresponds to a classical ferroelectric–paraelectric phase transition.[28] Fig. 5(c) shows the plots of $\ln(1/\varepsilon_r - 1/\varepsilon_m)$ vs $\ln(T - T_m)$ for the KNL–NTS ceramics with different ZnO contents. All samples exhibit relative good agreement with a linear relationship. The γ value was determined by least-squares fitting of the experimental data to this modified Curie–Weiss law and the results are plotted on the inset of Fig. 5(c).

For the undoped ceramics the calculated γ value is 1.37. As ZnO addition increases, γ increases gradually, see inset in Fig. 5(c), reaching a value of 1.59 for ZnO addition of 1.0 wt%, indicating that the ceramic evolved from a "normal ferroelectric state" towards a more relaxor state. The increase of γ value indicates the stabilization of a structure with local disorder and/or clusters that could be the cause of this relaxor behaviour for KNL–NTS. Therefore, the relaxor behaviour could be associated to the high disorder in A position[29] of the perovskite structure,

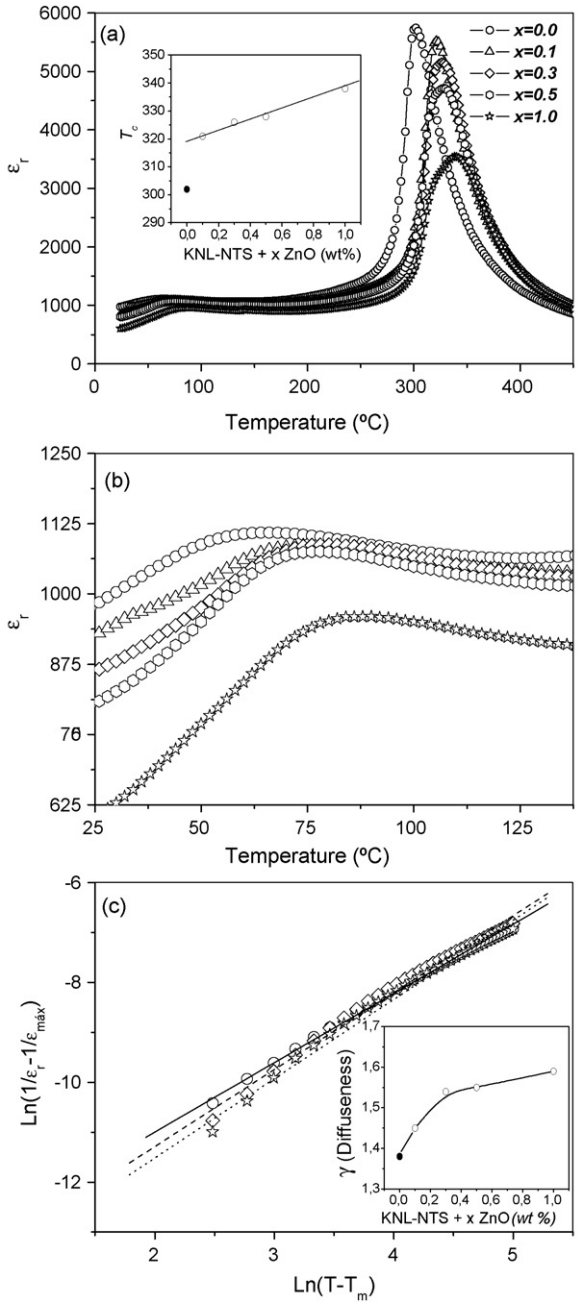

Fig. 5. (a) Temperature dependence of the dielectric constant (ε_r) of the KNL–NTS ceramics with different content of ZnO (wt%). The inset shows the evolution of the T_c as a function of the ZnO content. (b) Phase transition temperatures from orthorhombic to tetragonal phase ($T_{O–T}$) of the KNL–NTS ceramics with different content in ZnO. (c) $\ln(1/\varepsilon_r - 1/\varepsilon_m)$ vs $\ln(T - T_m)$ for the ceramics with ZnO contents of 0.0, 0.3 and 1.0 wt%. The symbols denote experimental data, while the solid lines correspond to the least-square fitting of the modified Curie–Weiss law. The inset shows the diffuseness, γ, of the ceramics as a function of the ZnO content.

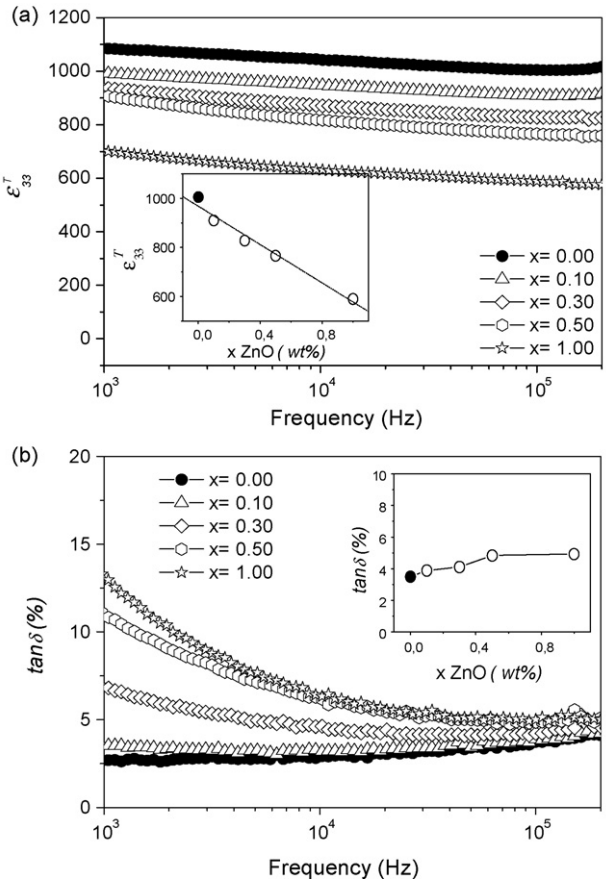

Fig. 6. (a) Dielectric constants and (b) dielectric losses as function of the frequency for KNL–NTS ceramics with different ZnO content. The inset of figure (a) shows the evolution of the dielectric constant at 100 KHz in the poled ceramics. The inset of figure (b) shows the evolution of the dielectric losses at 100 KHz in the poled ceramics.

as denoted by the increase in the diffusivity of the transition phase.

Fig. 6(a) and (b) show the room temperature dielectric properties of KNL–NTS poled ceramics at different frequencies. The ZnO addition provokes a linear decrease of the dielectric constant, see inset of Fig. 6(a), accompanied by a dielectric losses increase, especially at low frequencies. On the other hand, the response at high frequencies is only slightly affected by ZnO addition, as observed on the inset of Fig. 6(b). This reduction of the dielectric constant is in contrast to the results found on Zn-added KNN,[15] where an increase is observed for low ZnO concentrations, whereas a reduction is observed for high concentrations (over 3 mol%). This difference can be understood if we consider that the Zn^{2+} solubility limit is highly reduced in KNL–NTS in comparison to that in KNN. This different solubility limit would also explain the apparent divergences on the evolution of dielectric losses between both materials. On KNL–NTS an increase of dielectric losses is observed with the ZnO addition, whereas in KNN the dielectric losses remain unaltered for ZnO contents below the saturation point and increases for higher concentrations.

The reduction on the dielectric constant is a favourable result for power applications since it will reduce the capacitive effect of the piezoceramic actuator. The microstructural features observed seem to have a relevant role in the observed dielectric response. The phase coexistence introduces phase boundaries or defects that could be responsible for the increasing of the dielectric losses. The presence of secondary phase also accounts for

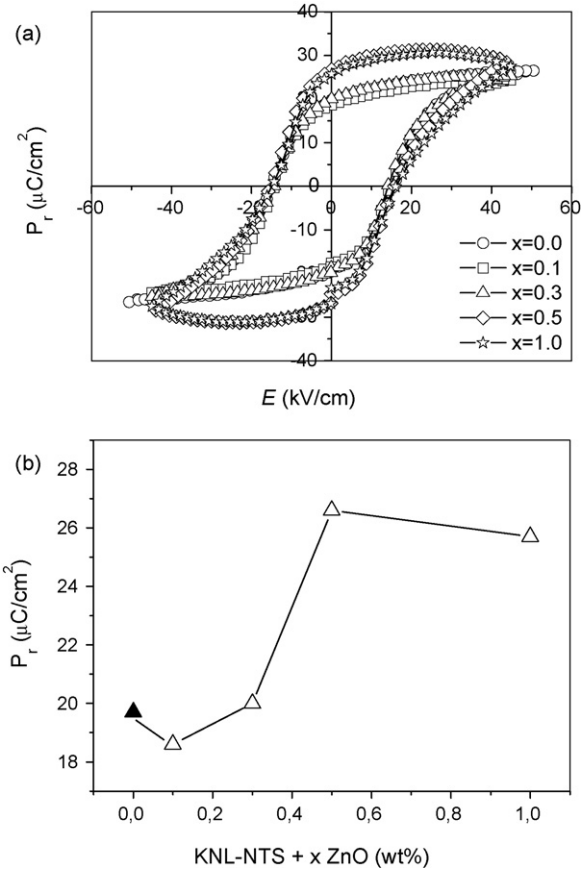

Fig. 7. (a) P–E hysteresis loops of KNL–NTS ceramics with different ZnO content and (b) the remanent polarization (Pr) as function of the amount of ZnO.

the decreasing of the dielectric constant and eventually changes the conductivity of the materials.

3.3. Ferroelectric and piezoelectric properties

Fig. 7(a) shows the P–E hysteresis loops of the ceramics with different ZnO content. The samples with ZnO content ≤0.3 wt% show hysteresis loops that are very similar to those of the undoped ceramics, whereas for higher ZnO contents an increase of the remanent polarization is observed, as shown in Fig. 7(b), where the remanent polarization (Pr) of the different samples is plotted. The undoped ceramic shows a large Pr (∼20 μC/cm^2) and a relatively large coercitive field, Ec (∼15.6 kV/cm). A small decrease of Ec occurs for low ZnO content, probably due to a decrease of the oxygen vacancies that pinned the domain wall motion. When KNL–NTS is modified by Zn^{2+} donor ions (A-site replacement), oxygen vacancies are reduced to keep the charge neutrality.[21] However, large ZnO contents ($x \geq 0.5$) produced a clear increase of the Pr together with a change on the shape of the hysteresis loops that could indicate the presence of conduction polarization in the samples.

Fig. 8 shows the dependences of the piezoelectric properties of the KNL–NTS ceramics on the ZnO content. As shown in Fig. 8, the d_{33} and k_p values for the undoped ceramic were 255 pC/N and 0.47, respectively (in good agreement with Ref. [22]). The d_{33} decreased gradually to a value of ∼100 pC/N for

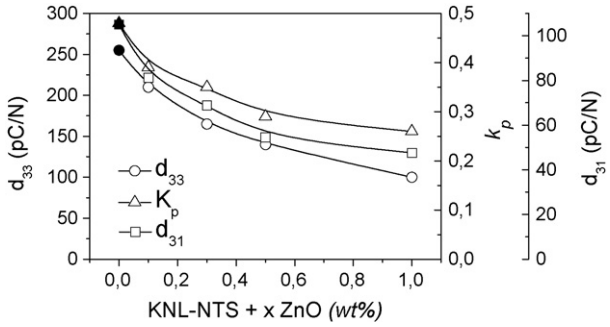

Fig. 8. Variations of the piezoelectric constants, d_{33}, d_{31}, and the electromechanical coupling factor (k_p) with the amount of ZnO in the KNL–NTS ceramics.

1.0 wt% ZnO addition. It is widely known that the piezoelectric constant, d_{33}, is approximately proportional to $\varepsilon^T{}_{33}$. Therefore, the decrease in d_{33} caused by ZnO-addition is considered to be associated with the decrease of $\varepsilon^T{}_{33}$ shown in the inset of Fig. 6(b). The same evolution with the ZnO content was observed in the electromechanical coupling factor (k_p) and piezoelectric constant, d_{31}.

Finally, Fig. 9 shows the evolution of the d_{33} values vs the tetragonality ratio for the different compositions studied in this work. A linear relationship was previously established[22] between the piezoelectric properties and the crystalline symmetry, represented by the tetragonality ratio. This linear dependence, also shown in Fig. 9, is due to the stabilization of the tetragonal phase at room temperature on behalf of the orthorhombic phase, i.e., due to the decrease of the polymorphism phase transition temperature of the samples. The piezoelectric constants of KNL–NTS ceramics doped with ZnO also show a linear dependence with the tetragonality ratio, but with a different slope regarding that of the undoped sample. The different slope could be explained by the increase in porosity and the generation of secondary phases, which would affect the piezoelectric constants and show no specific dependence with the tetragonality ratio.

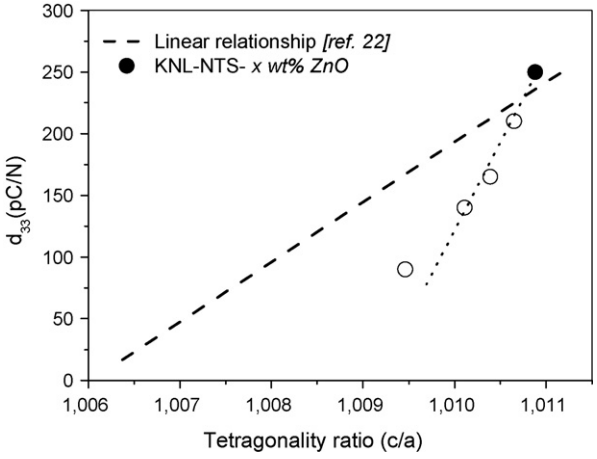

Fig. 9. Variations of the d_{33} as a function of the tetragonality ratio (*c*/*a*). The linear relationship obtained in Ref. [22] for KNL–NTS system is included for comparison.

4. Conclusions

In this study, the effect of ZnO addition on the structure, microstructure and electrical properties of KNL–NTS was investigated. At low ZnO doping levels (<0.3 wt%) the material is slightly modified and shows normal grains together with some abnormally grown grains. On the other hand, for ZnO doping levels ≥0.3 wt% a secondary phase with tetragonal tungsten–bronze structure is observed by XRD, accompanied by a great increase in the number and size of the abnormal grains. These grains show a complex structure, with a core of KNL–NTS subgrains showing different doping levels of Zn^{2+} and a partial shell of Zn-free material.

The ZnO doping produces an increase of the ferro-paraelectric phase transition temperature and a linear reduction of the room temperature dielectric constant of the material. These changes are accompanied by an increase of the orthorhombic to tetragonal morphotropic phase transition temperature. Conduction polarization processes are observed in highly doped samples.

A decrease of the piezoelectric coefficient is observed with the added quantity of ZnO. This reduction is related to the reduction of the tetragonality *c*/*a* ratio, produced by the increase of the morphotropic phase transition temperature.

Acknowledgments

The authors express their thanks to the CICYT project MAT2007-66845-C02-01 and to the MAGIN project PIF2006-60f0121 for their financial support. F. Rubio-Marcos thanks the FPI-CAM-FSE program for the research grant. Dr. J.J. Romero is indebted to CSIC for a "Junta de Ampliación de Estudios" contract (ref. JAEDOC087).

References

1. EU Directive 2002/95; <http://ec.europa.eu/environment/waste/weee/index_en.htm>.
2. Saito, Y., Takao, H., Tani, T., Nonoyama, T., Takatori, K., Homma, T. *et al.*, Lead-free piezoceramics. *Nature (London)*, 2004, **432**, 84–87.
3. Shrout, T. R. and Zhang, S. J., Lead-free piezoelectric ceramics: alternatives for PZT? *J. Electroceram.*, 2007, **19**, 111–124.
4. Kakimoto, K., Masuda, I. and Ohsato, H., Lead-free $KNbO_3$ piezoceramics synthesized by pressure-less sintering. *J. Eur. Ceram. Soc.*, 2005, **25**, 2719–2722.
5. Zhang, B., Li, J., Wang, K. and Zhang, H., Compositional dependence of piezoelectric properties in $Na_xK_{1-x}NbO_3$ lead-free ceramics prepared by spark plasma sintering. *J. Am. Ceram. Soc.*, 2006, **89**, 1605–1609.
6. Jaeger, E. and Egerton, L., Hot pressing of potassium sodium niobates. *J. Am. Ceram. Soc.*, 1962, **45**, 209–213.
7. Matsubara, M., Yamaguchi, T., Sakamoto, W., Kikuta, K., Yogo, T. and Hirano, S., Processing and piezoelectric properties of lead-free (K,Na)(NbTa)O_3 ceramics. *J. Am. Ceram. Soc.*, 2005, **88**, 1190–1196.
8. Takao, H., Saito, Y., Aoki, Y. and Hiribuchi, K., Microstructural evolution of crystalline-oriented $(K_{0.5}Na_{0.5})NbO_3$ piezoelectric ceramics with a sintering aid of CuO. *J. Am. Ceram. Soc.*, 2006, **89**, 1951–1956.
9. Zuo, R., Rödel, J., Chen, R. and Li, L., Sintering and electrical properties of lead-free $Na_{0.5}K_{0.5}NbO_3$ piezoelectric ceramics. *J. Am. Ceram. Soc.*, 2006, **89**, 2010–2015.
10. Bomlai, P., Sinsap, P., Muensit, S. and Milne, S. J., Effect of MnO on the phase development, microstructures, and dielectric properties of $0.95Na_{0.5}K_{0.5}NbO_3$–$0.05LiTaO_3$ ceramics. *J. Am. Ceram. Soc.*, 2008, **90**, 624–627.
11. Kosec, M. and Kolar, D., On activated sintering and electrical properties of $NaKNbO_3$. *Mater. Res. Bull.*, 1975, **50**, 335–340.
12. Ochoa, D. A., García, J. A., Pérez, R., Gomis, V., Albareda, A., Rubio-Marcos, F. *et al.*, Extrinsic contributions and nonlinear response in lead-free KNN-modified piezoceramics. *J. Phys. D: Appl. Phys.*, 2009, **42**, 025402.
13. Caballero, A. C., Fernández, J. F., Moure, C., Durán, P. and Chiang, Y. M., Grain growth control and dopant distribution in ZnO-doped $BaTiO_3$. *J. Am. Ceram. Soc.*, 1998, **81**, 939–944.
14. Kim, S.-J., Kang, C.-Y., Choi, J.-W., Kim, H.-J., Sung, M.-Y. and Yoon, S.-J., Low temperature sintering of ZnO-doped $0.01Pb(Mg_{1/2}W_{1/2})O_3$–$0.41Pb(Ni_{1/3}Nb_{2/3})O_3$–$0.35PbTiO_3$–$0.23PbZrO_3$ ceramics. *Jpn. J. Appl. Phys.*, 2007, **46**, 276–279.
15. Park, S.-H., Ahn, C.-W., Nahm, S. and Song, J.-S., Microstructure and piezoelectric properties of ZnO-added $(Na_{0.5}K_{0.5})NbO_3$ ceramics. *Jpn. J. Appl. Phys.*, 2004, **43**, 1072–1074.
16. Rubio-Marcos, F., Ochoa, P. and Fernandez, J. F., Sintering and properties of lead-free (K,NaLi)(Nb,Ta,Sb)O_3 ceramics. *J. Eur. Ceram. Soc.*, 2007, **27**, 4125–4129.
17. Malic, B., Jenko, D., Holc, J., Hrovat, M. and Kosec, M., Synthesis of sodium potassium niobate: a diffusion couples study. *J. Am. Ceram. Soc.*, 2008, **91**(6), 1916–1922.
18. Rodríguez-Carvajal, J., Recent developments of the program FULLPROF, in commission on powder diffraction (IUCr). *Newsletter*, 2001, **26**, 12–19, <http://journals.iucr.org/iucr-top/comm/cpd/Newsletters/>.
19. Tanaka, J., Onoda, Y., Tsukioka, M., Shimazu, M. and Ehara, S., The RMN study of Li ion motion in $K_3LiNb_6O_{17}$ and K_3LiTaO_{17}. *Jpn. J. Appl. Phys.*, 1981, **21**, 451–455.
20. Imai, K., Imaeda, M., Uda, S., Taniuchi, T. and Fukuda, T., Homogeneity and SHG properties of $K_3Li_{2-x}Nb_{5+x}O_{15+2x}$ single crystals grown by micro-pulling-down technique. *J. Cryst. Growth*, 1977, **177**, 79.
21. Li, E., Kakemoto, H., Wada, S. and Tsurumi, T., Influence of CuO on the structure and piezoelectric properties of the alkaline niobate-based lead-free ceramics. *J. Am. Ceram. Soc.*, 2007, **90**(6), 1787–1791.
22. Rubio-Marcos, F., Navarro-Rojero, M. G., Romero, J. J., Marchet, P. and Fernández, J. F., Piezoceramics properties as a function of the structure in the system (K,Na,Li)(Nb,Ta,Sb)O_3. *IEEE Trans. Ultrason. Ferroelectr. Freq. Control.*, in press.
23. Dai, Y., Zhang, X. and Zhu, G., Phase transitional behavior in $K_{0.5}Na_{0.5}NbO_3$–$LiTaO_3$ ceramics. *Appl. Phys. Lett.*, 2007, **90**, 262903.
24. Rubio-Marcos, F., Quesada, A., García, M. A., Bañares, M. A., Fierro, J. L. G., Martín-Gonzalez, M. S., Costa-Krämer, J. L. and Fernández, J. F., Some clues about the interphase reaction between ZnO and MnO_2 oxides. *J. Solid State Chem.*, 2009, **182**(5), 1211–1216.
25. Zhen, Y. and Li, J.-F., Abnormal grain growth and new core–shell structure in (K,Na)NbO_3-based lead-free piezoelectric ceramics. *J. Am. Ceram. Soc.*, 2007, **90**(11), 3496–3502.
26. Wang, Y., Damjanovic, D., Klein, N. and Setter, N., High-temperature instability of Li- and Ta-modified (K,Na)NbO_3 piezoceramics. *J. Am. Ceram. Soc.*, 2008, **91**, 1962–1970.
27. Uchino, K. and Nomura, S., Critical exponent of the dielectric constants in diffused phase transition crystal. *Ferroelectr. Lett. Sect.*, 1982, **44**, 55–61.
28. Smolensky, G. A., Physical phenomena in ferroelectrics with diffused phase transition. *J. Phys. Soc. Jpn.*, 1970, **28**(Suppl), 26–37.
29. Fernández, J. F., Caballero, A. C., Villegas, M., de Frutos, J. and Lascano, L., Relaxor behavior of $Pb_xBi_4Ti_{3+x}O_{12+3x}$ ($x = 2$, 3) aurivillius ceramics. *Appl. Phys. Lett.*, 2002, **81**, 4811.